High-resolution acoustic imaging at low frequencies using 3D-printed metamaterials

S. Laureti, D. A. Hutchins, L. A. J. Davis, S. J. Leigh, and M. Ricci

Citation: AIP Advances **6**, 121701 (2016); doi: 10.1063/1.4968606
View online: http://dx.doi.org/10.1063/1.4968606
View Table of Contents: http://scitation.aip.org/content/aip/journal/adva/6/12?ver=pdfcov
Published by the AIP Publishing

High-resolution acoustic imaging at low frequencies using 3D-printed metamaterials

S. Laureti,[1,2,a] D. A. Hutchins,[2,b] L. A. J. Davis,[1,c] S. J. Leigh,[1,d] and M. Ricci[2,e]
[1]*School of Engineering, University of Warwick, Library Road, Coventry, United Kingdom*
[2]*Department of Engineering, Polo Scientifico Didattico di Terni, University of Perugia, Strada di Pentima, Terni, Italy*

(Received 6 September 2016; accepted 21 October 2016; published online 23 November 2016)

An acoustic metamaterial has been constructed using 3D printing. It contained an array of air-filled channels, whose size and shape could be varied within the design and manufacture process. In this paper we analyze both numerically and experimentally the properties of this polymer metamaterial structure, and demonstrate its use for the imaging of a sample with sub-wavelength dimensions in the audible frequency range. [http://dx.doi.org/10.1063/1.4968606]

I. INTRODUCTION

Metamaterial research started in the field of optics, where it was noticed that a material containing regular forms of microstructure could be used to make a lens with a resolution greater than the normal diffraction limit. Acoustic metamaterials can also be designed and constructed, as firstly demonstrated in Refs. 1 and 2. The required behaviour is typically achieved by combining geometrical means and resonance effects – e.g. a conventional base material is modified so as to have a regular structure containing holes, channels, resonators or scattering sites – leading for example to a material exhibiting negative effective density (ρ_{EFF}) and bulk modulus (K_{EFF}), whereas normally they are both positive, resulting in a negative acoustic refractive index ($\eta_{EFF} < 0$).[3–5]

The ability to manipulate these fundamental properties makes the use of metamaterials highly interesting for acoustic applications in general and for ultrasonic imaging in particular, where there are applications ranging from diagnostic biomedical imaging to non-destructive evaluation (NDE). As an example, ultrasound is widely used to test industrial products such as concrete,[6,7] steel products[8,9] and plastics materials[10] so as to examine their internal structure. In all cases, the properties of the ultrasonic field determine the quality and resolution of the resulting image.

A negative refractive index metamaterial with flat, parallel surfaces is of interest in ultrasonic imaging because it can act as a lens and focus acoustic waves. However, it can do this at a greatly increased resolution than is possible using a conventional lens, by allowing the evanescent field carrying sub-wavelength information to be transmitted and focused on the other side of the lens.[11–13] Metamaterials thus give promise for improving the performance of biomedical ultrasound imaging and NDE, using their unique advantage: the resolution of the image is dictated by the fine structure of the metamaterial. The result is sub-wavelength resolution ultrasound imaging: a higher imaging resolution could be reached at the same inspection frequency. Alternatively, while keeping constant the resolution, lower frequencies could be used assuring an increased penetration into the body or into the sample under test.

[a]S.Laureti@warwick.ac.uk
[b]D.A.Hutchins@warwick.ac.uk
[c]Lee.Davis@warwick.ac.uk
[d]S.J.Leigh@warwick.ac.uk
[e]marco.ricci@unipg.it

Since the first experimental realizations of acoustic metamaterials, many different design strategies have been reported in the literature, although three general types can be considered:

(i) **Phononic crystals:** arrays of scatterers within the material create a 3D Bragg scattering effect.[14,15] The resultant negative index behaviour ($\eta_{EFF} < 0$) allows acoustic signals to be focused at particular frequencies at a resolution beyond the usual diffraction limit.[16]
(ii) **Channeled materials:** arrays of holes or channels through the thickness of the material create a set of Fabry-Peròt resonances, giving enhanced sub-wavelength imaging resolution by the coupling of evanescent waves.[17,18]
(iii) **Space coiling:** spiral paths within a material lead to focusing effects and the possibility of negative refraction properties ($\eta_{EFF} < 0$).[19–21]

There are some aspects of the above metamaterial structures that need to be investigated further if acoustic metamaterials are to be used for acoustic imaging applications. Zhu et al.[17] demonstrated that a holey structured metamaterial of 40x40 holes realized in brass can be utilized for the imaging of an object having dimension up to $\lambda/50$ at a frequency of 2.18 kHz in air. This represents the current state-of-the-art for the use of such acoustic metamaterial in air for imaging a sub-wavelength object. It was also shown theoretically that polymers could be used to realize acoustic metamaterial devices.[22] Thus, the use of 3D printing potentially allows the fabrication of acoustic metamaterials whose internal construction could be varied to provide broad-bandwidth operation at ultrasonic frequencies. Following the work of Zhu *et al.*[17] and Laureti *et al.*,[23] the present paper describes the properties of a 3D-printed acoustic metamaterial containing 100 channels, using both numerical simulation and experiment. This metamaterial is then used to image a sub-wavelength object in air.

II. THEORETICAL BACKGROUND

A study by Christensen *et al.*[24] demonstrated the action of a 2D array of square-shaped holes within a bulk material. The results showed that Fabry-Peròt resonances (FPRs) existed within these holes, the frequency peak positions of which was related to the thickness h of the metamaterial. Furthermore, FPRs could be excited by very large wave vectors k which carry sub-wavelength information. This is the key-point that needed to be understood in order to gain insight into the operation of holey structured acoustic metamaterials.

In order to understand better how holey metamaterials help in coupling the evanescent field scattered from an object of sub-wavelength dimensions, we follow the same formalism utilized Zhu *et al.* We consider henceforth the effective medium limit approximation, that is when the wavelength of the impinging plane wave λ is much larger than the channel's lattice constants a and Λ (a being the lateral dimension of the square-shaped hole and Λ the lattice parameter (or center-to-center distance, see Fig. 1). In this condition, propagation within the holes via FPRs dominates

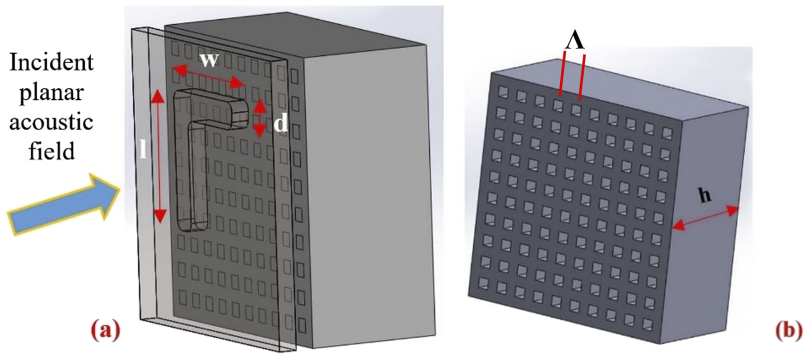

FIG. 1. (a) L-shaped aperture with dimensions l = 20 mm; w = 20 mm; d = 3 mm, held against a 1.5 mm thick aluminium slab. (b) Acoustic metamaterial with h = 14.8mm, containing 1.48mm wide square-sided holes, with their centres separated by 2.96mm (Λ). There was a 2 mm gap between the plate and the metamaterial.

the acoustic energy transmission process. The probability of the plane wave of parallel momentum $\vec{k}_{\|} = (k_x, k_y)$ to be transmitted to the other side of the metamaterial in a diffracted plane wave with $\vec{k}_{\|}^{(n,p)} = \left(\frac{k_x+n2\pi}{\Lambda}, \frac{k_y+p2\pi}{\Lambda}\right)$, it is expressed by the transmission coefficient t:

$$t^{np}\left(\lambda, \vec{k}_{\|}\right) = -S_{np}v', \tag{1}$$

where S_{np} is the overlap integral between the diffracted wave of order *(n,p)*, $v' = \frac{I_0 G_v}{(G-\Sigma)^2 - G_v^2}$.

The term I_0 is proportional to the overlap integral between the incident wave and the fundamental mode, S_{00}, where $I_0 = 2iS_{00}$. G_v and Σ depend on the propagation constant of the fundamental mode k_0, and on the thickness h of the acoustic metamaterial:

$$\Sigma = \frac{cosk_0h}{sink_0h} \tag{2}$$

$$G_v = \frac{1}{sink_0h}$$

The G terms that takes the coupling between neighboring holes into account are expressed as a sum of diffracted modes:

$$G = i\sum_{lm}\frac{k_0}{k_z^{(l,m)}}|S_{lm}|^2 \tag{3}$$

where $k_z^{(l,m)} = \sqrt{k_0^2 - \left[\vec{k}_{\|}^{(l,m)}\right]^2}$.

It can be seen that the first term of the above sum, (l=m=*0*), is dominant and thus $G = iY|S_{00}|^2$, where $Y = \frac{k_0}{\sqrt{k_0^2 - k_f^2}}$. By substituting all these quantities into equation (1), we obtain:

$$t^{00}\left(\lambda, \vec{k}_{\|}\right) = \frac{4|S_{00}|^2 Ye^{iq_zh}}{\left(1 + Y|S_{00}|^2\right)^2 - \left(1 - Y|S_{00}|^2\right)^2 e^{2iq_zh}} \tag{4}$$

For wavelengths corresponding to a FPR, $\lambda_R = \frac{2h}{m}$, reduces to:

$$t^{00}\left(\lambda_R, \vec{k}_{\|}\right) = (-1)^m \tag{5}$$

This is valid for all values of $\vec{k}_{\|}$. This means that, at the resonance condition, even those values associated with evanescent waves (which carry sub-wavelength details) are successfully transferred to the outer side of the metamaterial, and can contribute to imaging. This is the key point in understanding the working principle of holey-structured acoustic metamaterials: they allow the near field region of the acoustic field to be transferred over distances at which it would not normally be possible to be observed.

III. ACOUSTIC METAMATERIAL DESIGN AND EXPERIMENTAL SETUP

The acoustic metamaterial device presented in this work has been realized by 3D printing additive manufacturing using PMMA photo-polymer. The metamaterial itself was manufactured with a uniform array of through-thickness square holes. Thickness h has been chosen to be 14.8 mm, giving a nominal fundamental frequency of 11.48 kHz in air, but allowing operation of integer multiples of this value. It contains 1.48 mm wide square-sided holes, with their centers separated by $\Lambda = 2.96$ mm (which determines the maximum achievable resolution[11]).

The metamaterial was used to image both an L-shaped and a T-shaped aperture, both machined into a 1.5 mm thick aluminum slab, as shown in Figures 1(a) and 4(a). The width d of these two apertures is significantly smaller than the wavelength range of inspection and almost coincides with the lattice parameter Λ, so as to test whether the imaging resolution can reach the single-hole limit.

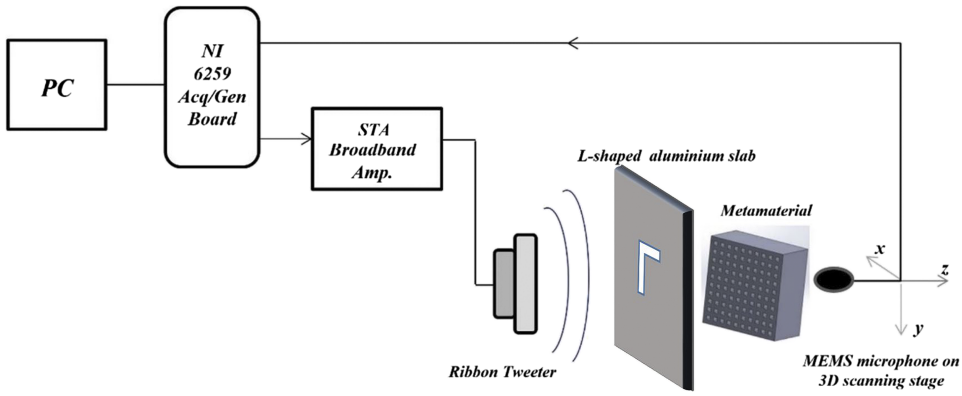

FIG. 2. Sketch of the experimental setup.

A planar acoustic field was incident onto the sample, and the signal transmitted through the structure in air subsequently imaged on the far side at selected frequencies. Note that it was noted that transmission and imaging performance could take place across a range of frequencies, outside the nominal design frequency, as will be demonstrated below. The dimensions of the specimen and metamaterial are shown in Figure 1. It is important to consider the experimental design carefully. This is because it is difficult to find a plane wave acoustic source with a flat response over the required frequency range. In addition, the dimensions of the receiver should be smaller than that of the holes to avoid spatial averaging of the acoustic field. For acoustic generation, a MONACOR RBT 20 ribbon tweeter was used for the acoustic generation, together with a STA-225 broadband amplifier. A waveguide with its walls covered by absorbing material was used to obtain a flat and homogenous excitation acoustic field impinging over the sample. The signal generation/acquisition was managed by a National Instrument 6259 board connected to a PC. In previous work described in the literature, the microphone dimensions have been larger than that of a single hole; this implies that a deconvolution algorithm had to be applied to the reconstructed images to counterbalance the degradation of resolution due to the microphone dimensions. To mitigate this effect, we have used a MEMS microphone with a sensitive area of 0.25 mm of diameter, much smaller than the hole dimensions, which allows the collection of at least five discrete measurement points across each hole. The drawback of using such a small device MEMS is that its sensitivity is not very high, leading to noisy measurements, and moreover its spectrum is not flat in the frequency region of interest exhibiting a peak around 15 kHz. Therefore each recorded signal was normalized in the frequency domain with respect to the MEMS reference spectrum.

A 3D -motorized scanning stage moved a microphone to measure the pressure field across 2D planes perpendicular to the acoustic propagation axis at the far side of the metamaterial. A schematic diagram of the experimental setup is depicted in Figure 2:

The tweeter was driven by a swept-frequency chirp signal over a pre-defined frequency range. This technique was used with acoustic metamaterials so as to be able to exploit advanced post-processing algorithms.[25] Data acquisition was performed using a series of stepped x-y scans of the acoustic field amplitude, which was acquired at different distances z from the outer surface of the metamaterial (see Figure 2). Each acquired signal was smoothed using a moving averages method and analyzed in the frequency domain using a Z-Transform algorithm. This allows the retrieved acoustic field to be analyzed in a specific set of frequencies with respect to the standard Fast Fourier Transform algorithm.[26,27]

IV. SUB-WAVELENGTH IMAGING EXPERIMENTAL RESULTS AND FEM SIMULATIONS

The sample in the form of the "L" shaped aperture in the aluminum plate was placed 2 mm away from the metamaterial input surface, and the output field was collected in air at distances of z = 0.5 and z = 1 mm from the outer surface. The resulting distance between the sample and the MEMS microphone receiver was thus ~18mm.

The experimental results are shown in Figures 3 (a) and 3 (b), where the amplitude recorded at the outer metamaterial surface is plotted as a function of position at various frequencies in the 9.8 – 10.3 kHz range. It can be seen that the L-shaped aperture has been recovered well over a range of frequencies in both cases. In particular for z = 0.5mm the holey pattern can be clearly observed superimposed to the "L" image. This agrees with that reported in Ref. 17 - supplementary information.

A Finite Element model has also been developed using COMSOL®, using the frequency-domain analysis into the acoustic module. Default values have been used for densities and sound velocities of both air and PMMA. The L-shaped aperture was assumed to be 2 mm away from the metamaterial surface and a planar acoustic pressure field impinges the aperture, as shown in Figure 1(a). The acoustic field predicted above the other side of the metamaterial is shown in Figure 3 (c). Results are shown at 10 kHz for several distances from the metamaterial outer surface. As in the experiment, a clear image is predicted.

In order to further validate the results achieved on the imaging of a sub-wavelength dimension aperture, here another example of holey-structured acoustic metamaterial capabilities is reported. In this case, a 2 mm aluminium slab has been crafted to have a "T" shaped aperture, whose dimensions are shown in Figure 4(a). Both arms of the "T" are 20 mm long, whilst its width d is 3 mm. As for

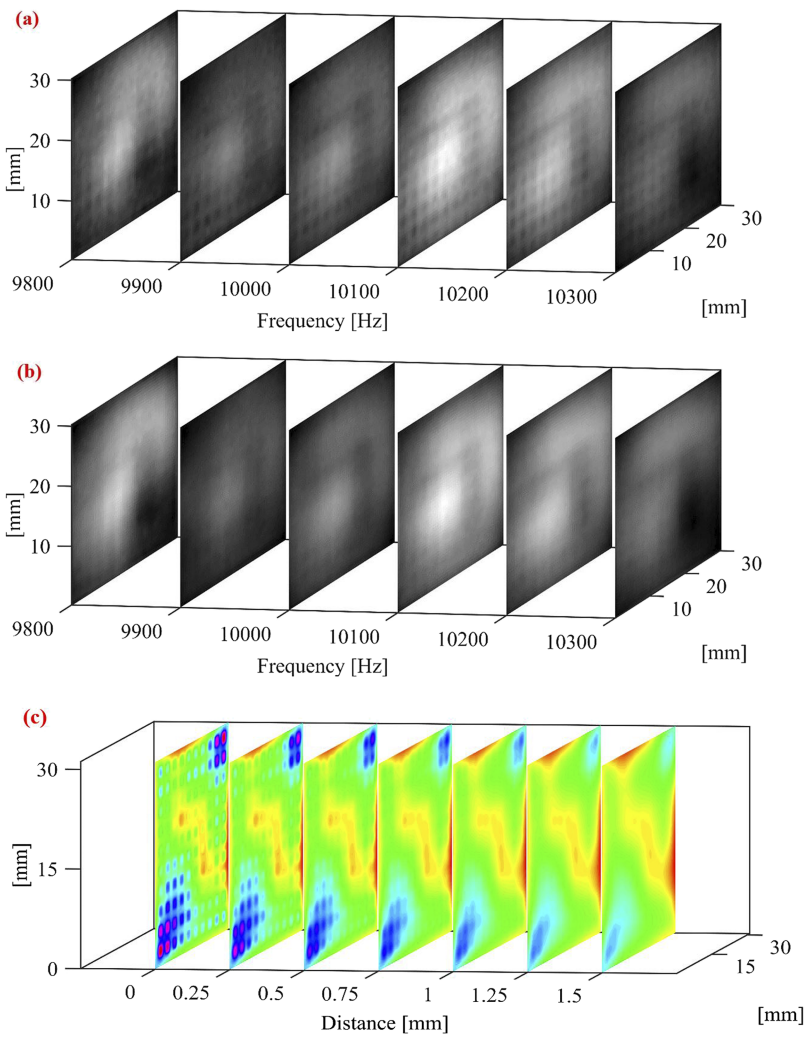

FIG. 3. Experimental results at (a) 0.5 mm and (b) 1 mm from the metamaterial surface. (c) FEM results at several distances from the metamaterial surface, frequency 10 kHz.

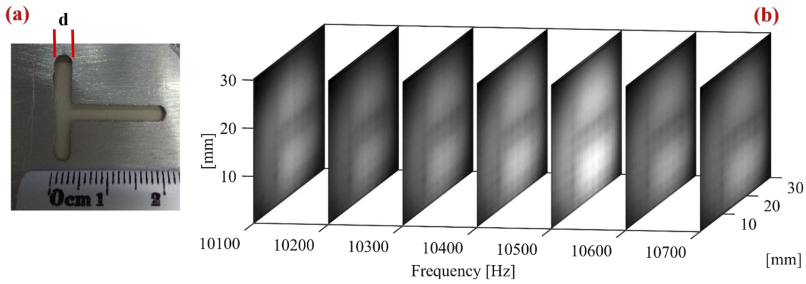

FIG. 4. (a) "T" shaped aluminium slab dimensions. (b)"T" Experimental results at 0.5 mm from the metamaterial surface.

the "L" case described above, Figure 4(b) shows the acoustic field retrieved at the outer metamaterial surface as a function of frequency. It can be seen that the "T" shaped aperture with subwavelength dimensions has again been imaged clearly using the holey-structured acoustic metamaterial device, over the range of frequencies quoted.

V. TOWARD THE REALIZATION OF AN ACOUSTIC BROAD-BAND DEVICE

Coded waveforms such as chirps or bipolar sequences can be used to enhance the range of acoustic frequencies that are transmitted through materials, and have been used in many materials studies where signals are embedded in noise.[28] They are thus of interest here. In order to exploit acoustic metamaterials in practical applications, one has to face the fact that they usually operate over a narrow bandwidth and at relatively low frequencies; this is due to the current sizes and nature of the structural features within them. An acoustic metamaterial with the ability to restore the evanescent field into a broadband frequency range is needed for working on real applications, especially in the ultrasonic region for ultrasonic non-destructive testing applications and medical imaging. To achieve operation at much higher frequencies, advances over current practice are needed:

- The internal structures will need to be formed in much finer detail than at present;
- Metamaterials will need to have broad bandwidth capability;
- Acoustic coupling into and out of many metamaterials is inefficient due to their design, and needs to be improved;

L.Zigoneanu *et al.*[29] demonstrated that a pyramidal acoustic metamaterial geometry can be used to broaden the cloaking effect of an acoustic metamaterial. A similar approach has been used here to extend number of frequencies within an input signal that satisfies Equation (5), namely when $\lambda = \frac{2h}{m}$, hence $f = m\frac{c}{2h}$ with m positive and integer and c the speed of sound of the air. Therefore,

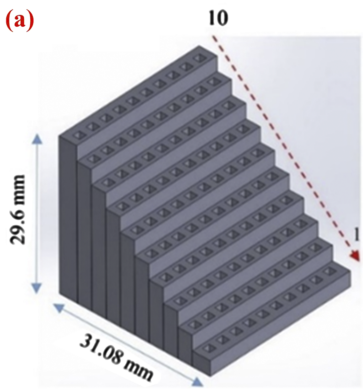

(b)

Step Number	Expected Resonance Frequency (Hz)
1	57939
2	28970
3	19313
4	14485
5	11588
6	9656
7	8277
8	7242
9	6437
10	5793

FIG. 5. (a) "Stepped" acoustic metamaterial design dimensions; (b) expected FPR frequency in air for each step change in thickness.

a metamaterial constructed so as to have with finite increments in its thickness h should provide a higher number of resonance frequency conditions, and hence transmit a wider bandwidth of signal. A sketch of the 3D-printed acoustic metamaterial containing such "Steps" is shown in Figure 5(a).

This metamaterial has a squared base, and has ten finite increments in height of 2.96 mm each, which are here called for simplicity "steps". It contains a hundred squared-side holes of 1.48 mm lateral dimension, so as to obtain results comparable to the constant thickness acoustic metamaterial described above. Figure 5(b) shows the fundamental frequency expected from FPRs at each incremental step change in thickness. It should also be noted that every integer multiple of this set of frequencies it is a valid value to obtain another resonance.

The experimental results are shown in Figure 6, where again an x-y planar scan of the acoustic field at the outer surface of the metamaterial is reported. Each figure subplot highlights the frequency where each step reaches its resonance condition. Please note that figures start from the results obtained for step number 10 to step number 2, so as to have the frequencies of resonance increasing as shown. Step number 1, whose resonance frequency is expected to be at 57.9 kHz it not reported because it is outside the frequency range of measurement using the present experimental setup.

The expected behaviour is observed, with transmission intensity increased at certain frequencies and sample thickness, as observed by the lines of brighter lines dots across the images. Note that there are some differences between the observed resonance frequency and the one predicted theoretically. This is thought to be due to various factors such as the limited sensitivity of the MEMS microphone, the resolution of the Z-Transform algorithm used for data analysis, and variations in room temperature (and hence also of sound velocity in air).

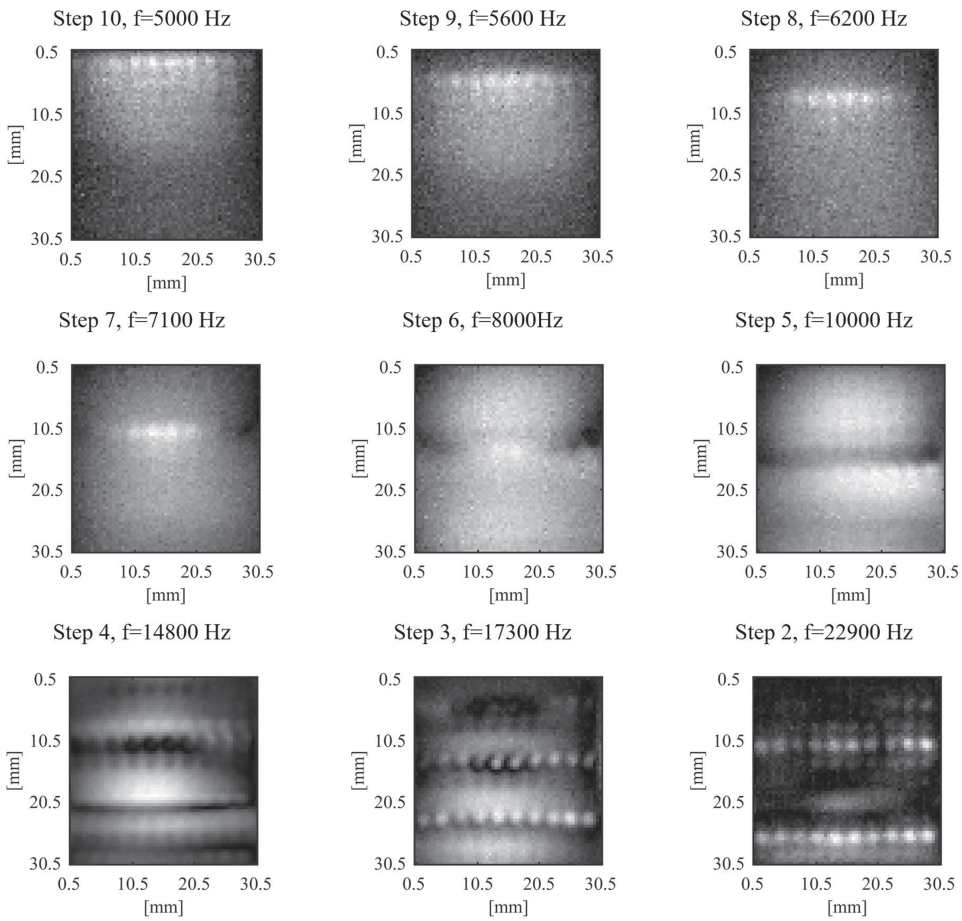

FIG. 6. Intensity plots over x-y planes at a fixed distance from the "stepped" acoustic metamaterial device for several different frequencies. Each subplot highlights the frequency and the corresponding step where the resonance condition is achieved.

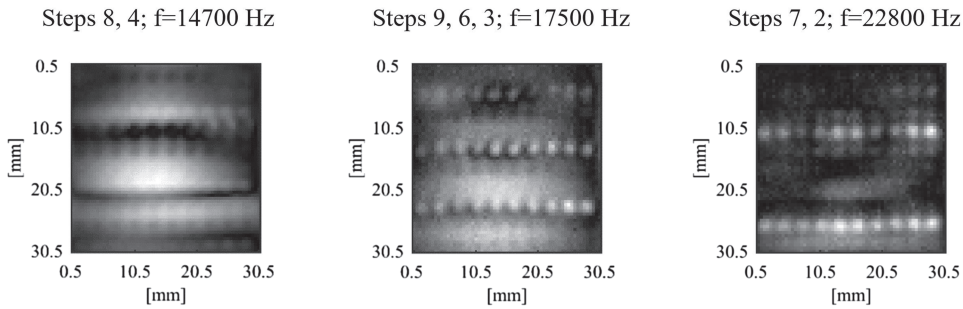

FIG. 7. x-y planes at a fixed distance from the "stepped" acoustic metamaterial device for several different frequencies. Each subplot highlights the frequency and the corresponding steps where the resonance condition is achieved.

As might be expected, the resonance condition can be reached by different steps for the same impinging frequencies, provided the thickness and frequencies match in each case. The set of resonance frequencies $f_n^{(s)}$ of the s^{th} step can be expressed as:

$$f_n^{(s)} = n\frac{cN_s}{2(s \times h)} \tag{6}$$

where n is the integer number associated to the n^{th} resonance mode of the s^{th} step and $\frac{s \times h}{N_s}$ is the step length.

It follows that different steps s, s' could have common resonance frequencies for different resonance modes n, n' when the following condition is satisfied:

$$\frac{n}{s} = \frac{n'}{s'} \rightarrow \frac{n}{n'} = \frac{s}{s'} \tag{7}$$

As an example of multiple matched condition observed, subplots within Figure 7 shows three example of channels resonating together.

VI. CONCLUSIONS

It has been demonstrated that 3D-printed metamaterials can be used for sub-wavelength acoustic imaging in air. The fabrication technique allows different metamaterial structures to be designed and constructed. In the first design, using a material with constant thickness, it was shown that the expected image resolution could be obtained over a limited range of frequencies, over which the FPR existed in the holes of constant thickness. A change in thickness across the metamaterial was also examined, and a range of resonant frequencies observed as increased transmission intensities. This stepped material was able to transmit signals at a set of discrete frequencies, ranging from 5 kHz to 22.9 kHz. This demonstrates the first steps towards a broad bandwidth device, which could incorporate these and other design features available in 3D printing to develop metamaterials with properties that could be used in real acoustic imaging applications.

[1] X. Zhang and Z. Liu, "Negative refraction of acoustic waves in two-dimensional phononic crystals," Appl. Phys. Lett. **85**(2), 341–343 (2004).
[2] S. Yang, J. Page, Z. Liu, M. Cowan, C. Chan, and P. Sheng, "Focusing of sound in a 3D phononic crystal," Phys. Rev. Lett. **93**(2), 24301 (2004).
[3] V. G. Veselago, "The electrodynamics of substances with simultaneously negative values of ε and μ," Physics-Uspekhi **10**(4), 509–514 (1968).
[4] J. B. Pendry, "Negative refraction makes a perfect lense," Phys. Rev. Lett. **85**(18), 3966 (2000).
[5] D. R. Smith, J. B. Pendry, and M. C. K. Wiltshire, "Metamaterials and negative refractive index," Science **305**(5685), 788–92 (2004).
[6] S. Ould Naffa, M. Goueygou, B. Piwakowski, and F. Buyle-Bodin, "Detection of chemical damage in concrete using ultrasound," Ultrasonics **40**(1–8), 247–251 (2002).
[7] P. Purnell, T. H. Gan, D. A. Hutchins, and J. Berriman, "Noncontact ultrasonic diagnostics in concrete: A preliminary investigation," Cem. Concr. Res. **34**(7), 1185–1188 (2004).
[8] S. E. Burrows, A. Rashed, D. P. Almond, and S. Dixon, "Combined laser spot imaging thermography and ultrasonic measurements for crack detection," Ndte **22**(2–3), 217–227 (2007).

[9] M. Ricci, L. Senni, P. Burrascano, R. Borgna, S. Neri, and M. Calderini, "Pulse-compression ultrasonic technique for the inspection of forged steel with high attenuation," Insight: Non-Destructive Testing and Condition Monitoring **54**(2), 91–95 (2012).
[10] D. E. W. Stone and B. Clarke, "Ultrasonic attenuation as a measure of void content in carbon-fibre reinforced plastics," Non-Destructive Test. **8**(3), 137–145 (1975).
[11] J. Jung, F. García-Vidal, L. Martín-Moreno, and J. Pendry, "Holey metal films make perfect endoscopes," Phys. Rev. B **79**(15), 153407 (2009).
[12] J. B. Pendry, D. Schurig, and D. R. Smith, "Controlling electromagnetic fields," Science **312**(5781), 1780–1782 (2006).
[13] S. Zhang, Y.-S. Park, J. Li, X. Lu, W. Zhang, and X. Zhang, "Negative refractive index in chiral metamaterials," Phys. Rev. Lett. **102**(2), 23901 (2009).
[14] S. Yang, J. H. Page, M. L. Cowan, C. T. Chan, and P. Sheng, "Phononic crystals," La Phys. au Canada 187–189 (2001).
[15] C. Charles, B. Bonello, and F. Ganot, "Propagation of guided elastic waves in 2D phononic crystals," Ultrasonics **44**(SUPPL.), (2006).
[16] A. Sukhovich, L. Jing, and J. H. Page, "Negative refraction and focusing of ultrasound in two-dimensional phononic crystals," Phys. Rev. B - Condens. Matter Mater. Phys. **77**(1), (2008).
[17] J. Zhu, J. Christensen, J. Jung, and L. Martin-Moreno, "A holey-structured metamaterial for acoustic deep-subwavelength imaging," Nat. Phys. **7**(1), 52–55 (2011).
[18] H. Su, X. Zhou, X. Xu, and G. Hu, "Experimental study on acoustic subwavelength imaging of holey-structured metamaterials by resonant tunneling," J. Acoust. Soc. Am. **135**(4), 1686 (2014).
[19] Z. Liang and J. Li, "Extreme acoustic metamaterial by coiling up space," Phys. Rev. Lett. **108**(11), (2012).
[20] Z. Liang, T. Feng, S. Lok, F. Liu, K. B. Ng, C. H. Chan, J. Wang, S. Han, S. Lee, and J. Li, "Space-coiling metamaterials with double negativity and conical dispersion," Sci. Rep. **3**, 1614 (2013).
[21] Y. Xie, A. Konneker, B. I. Popa, and S. A. Cummer, "Tapered labyrinthine acoustic metamaterials for broadband impedance matching," Appl. Phys. Lett. **103**(20), (2013).
[22] H. Estrada, P. Candelas, A. Uris, F. Belmar, F. J. García De Abajo, and F. Meseguer, "Extraordinary sound screening in perforated plates," Phys. Rev. Lett. **101**(8), (2008).
[23] S. Laureti, L. A. J. Davis, M. Ricci, and D. A. Hutchins, "The study of broadband acoustic metamaterials in air," in Ultrasonics Symposium (IUS), 2014 IEEE International, 2014, pp. 1344–1347.
[24] J. Christensen, "Theory of resonant acoustic transmission through subwavelength apertures," Phys. Rev. Lett. **101**(1), 14301 (2008).
[25] D. Hutchins, P. Burrascano, L. Davis, S. Laureti, and M. Ricci, "Coded waveforms for optimised air-coupled ultrasonic nondestructive evaluation," Ultrasonics (2014).
[26] L. Rabiner, R. Schafer, and C. Rader, "The chirp x-transform algorithm," IEEE Trans. Audio Electroacoust. **17**(2), 86–92 (1969).
[27] L. Rabiner and R. Schafer, "The chirp z-transform algorithm and its application," Bell Syst. Tech. (1969).
[28] P. Pallav, T. H. Gan, and D. A. Hutchins, "Elliptical-tukey chirp signal for ultrasonic imaging," IEEE Trans. Ultrason. Ferroeletrics, Freq. Control **54**(8), 1530–1540.
[29] L. Zigoneanu, B. Popa, and S. A. Cummer, "Three-dimensional broadband omnidirectional acoustic ground cloak," Nat. Mater. **13**, 1–4 (2014).